

# Dark Matter Search Using *Chandra* Observations of Willman 1, and a Spectral Feature Consistent with a Decay Line of a 5 keV Sterile Neutrino

Michael Loewenstein<sup>1,2</sup>, Alexander Kusenko<sup>3,4</sup>

## ABSTRACT

We report the results of a search for an emission line from radiatively decaying dark matter in the *Chandra* X-ray Observatory spectrum of the ultra-faint dwarf spheroidal galaxy Willman 1. 99% confidence line flux upper limits over the 0.4-7 keV *Chandra* bandpass are derived and mapped to an allowed region in the sterile neutrino mass-mixing angle plane that is consistent with recent constraints from *Suzaku* X-ray Observatory and *Chandra* observations of the Ursa Minor and Draco dwarf spheroidals. A significant excess to the continuum, detected by fitting the particle-background-subtracted source spectrum, indicates the presence of a narrow emission feature with energy  $2.51 \pm 0.07(0.11)$  keV and flux  $[3.53 \pm 1.95(2.77)] \times 10^{-6}$  photons  $\text{cm}^{-2} \text{s}^{-1}$  at 68% (90%) confidence. Interpreting this as an emission line from sterile neutrino radiative decay, we derive the corresponding allowed range of sterile neutrino mass and mixing angle using two approaches. The first assumes that dark matter is solely composed of sterile neutrinos, and the second relaxes that requirement. The feature is consistent with the sterile neutrino mass of  $5.0 \pm 0.2$  keV and a mixing angle in a narrow range for which neutrino oscillations can produce all of the dark matter and for which sterile neutrino emission from the cooling neutron stars can explain pulsar kicks, thus bolstering both the statistical and physical significance of our measurement.

---

<sup>1</sup>Department of Astronomy, University of Maryland, College Park, MD.

<sup>2</sup>CRESST and X-ray Astrophysics Laboratory NASA/GSFC, Greenbelt, MD.

<sup>3</sup>Department of Physics and Astronomy, University of California, Los Angeles, CA 90095-1547, USA

<sup>4</sup>Institute for the Physics and Mathematics of the Universe, University of Tokyo, Kashiwa, Chiba 277-8568, Japan

## 1. Introduction

### 1.1. Context

None of the Standard Model particles can account for the dark matter that makes up most of the mass in the universe. We report the latest results of a search for dark matter in the form of relic sterile neutrinos (see Kusenko 2009 for an up-to-date review). The motivation for considering the sterile neutrino, one of a number of feasible dark-matter candidates, is two-fold. First, the discovery of ordinary neutrino masses is most easily accommodated by means of the so-called seesaw mechanism, which calls for some new gauge-singlet fermions. If all of these fermions have very large Majorana masses, there are no additional degrees of freedom (particles) at the low energy scale. However, if one of these mass parameters lies in the 1–30 keV range, the corresponding *sterile* neutrino can be the long sought-after dark matter particle (Dodelson & Widrow 1994). Second, the physics of supernovae, that often assists in ruling out hypothetical low-mass particles, provides some intriguing clues in favor of the existence of sterile neutrinos with the same parameters that are required to explain dark matter. Such particles would be anisotropically emitted from a cooling newly born neutron star, inducing a sufficient recoil momentum in the neutron star to explain the observed velocities of pulsars (Kusenko & Segrè 1997; Fuller et al. 2003). X-ray observations offer the best probe of this well-motivated dark-matter candidate (Kusenko 2009). In the early universe, sterile neutrinos may be produced through non-resonant oscillations (Dodelson & Widrow 1994), resonant oscillations (Shi & Fuller 1999) and via various other channels (Kusenko 2006; Shaposhnikov & Tkachev 2006; Petraki & Kusenko 2008). The kinetic properties of dark matter relevant for structure formation on small scales (i.e., how “warm” or “cold” the dark matter is) depend on the production scenario, as well as the particle mass (Kusenko 2006; Petraki 2008; Boyanovsky 2008b).

The generic prediction is that relic sterile neutrinos must decay into a lighter neutrino and a photon (Pal & Wolfenstein 1982). Since this two-body decay of a 1–30 keV mass particle produces a narrow line with energy  $E_\gamma = m_{\text{st}}c^2/2$ , X-ray astronomy provides a unique opportunity to discover these relic particles. Archival X-ray data has been used to set limits on relic sterile neutrinos (see the review in Kusenko 2009). In addition, a dedicated search for sterile neutrinos using the *Suzaku* X-ray telescope has recently been conducted by Loewenstein, Kusenko, & Biermann (2009) (hereafter, LKB). Here we will present new results from the search using the *Chandra* X-ray Observatory. Our analysis of data on the Willman 1 dwarf spheroidal galaxy yields evidence of a 2.5 keV line, consistent with the decay of a relic sterile neutrino with mass 5 keV; and, with an inferred line strength consistent with that expected if all of the dark matter is composed of sterile neutrinos produced by oscillations.

## 1.2. Target selection

Given the uncertainty in sterile neutrino properties, and the importance of dark matter discovery, one ought to explore the X-ray band with existing instruments using well-chosen targets. While the decay timescale greatly exceeds the Hubble time (Pal & Wolfenstein 1982; Barger et al. 1995), the emissivity may reach detectable levels in regions of large dark matter surface density, such as galaxy clusters, M31, and Local Group dwarf spheroidal galaxies (Abazajian et al. 2001a,b; Dolgov & Hansen 2002; Boyarsky et al. 2006). The last offer, arguably, the most promising opportunity because of the proximity and high dark matter density in these systems, and the absence of additional competing internal X-ray sources. *Suzaku* Observing Cycle 2 observing time was awarded time to study the best available targets at that time: the Ursa Minor and Draco dwarf spheroidals (LKB). Subsequently, a new sub-population of faint Milky Way satellites discovered in the Sloan Digital Sky Survey (SDSS) were found to have very high mass-to-light ratios (Strigari et al. 2008a; Walker et al. 2009). These rival or surpass Ursa Minor and Draco as compelling targets for sterile neutrino searches. We were awarded 100 ks of observing time in *Chandra* cycle 10 to investigate one of these – namely Willman 1. These data represent the first X-ray observations of this extreme system; and, we report on our findings here.

## 1.3. Previous Results on Ursa Minor

The basic equations relating the galaxy parameters (distance  $100d_{100}$  kpc, dark matter mass in projection  $M_{\text{pro}} = 10^7 M_7 M_\odot$ ), X-ray observables (line energy  $E_\gamma$ , line flux  $F_{\text{line}}$ ), and sterile neutrino parameters (mass  $m_{\text{st}}$ , mixing angle  $\theta$ , fraction of dark matter in sterile neutrinos  $f_{\text{st}}$ ), are the following (Loewenstein et al. 2009, Kusenko 2009, and references therein):

$$m_{\text{st}} = 2E_\gamma, \quad (1)$$

$$\Gamma_{\nu_s \rightarrow \gamma \nu_a} = 5.52 \times 10^{-32} \left( \frac{\sin^2 \theta}{10^{-10}} \right) \left( \frac{m_{\text{st}}}{\text{keV}} \right)^5, \quad (2)$$

and

$$F_{\text{line}} = 4.69 \times 10^{-6} \Gamma_{-27} f_{\text{st}} M_7 d_{100}^{-2} \left( \frac{\text{keV}}{E_\gamma} \right) \quad (3)$$

$$= 5.15 \times 10^{-10} \left( \frac{\sin^2 \theta}{10^{-10}} \right) \left( \frac{m_{\text{st}}}{\text{keV}} \right)^4 f_{\text{st}} M_7 d_{100}^{-2} \text{ photons cm}^{-2} \text{ s}^{-1}. \quad (4)$$

The abundance of sterile neutrinos produced through non-resonant oscillations may be calculated for given values of  $m_{\text{st}}$  and  $\theta$ , assuming the standard early thermal history of the

universe. This relation determines  $f_{\text{st}}$  as a function of  $m_{\text{st}}$  and  $\theta$ , assuming that all sterile neutrinos are produced in this way as first proposed by Dodelson & Widrow (1994), and lower limits on  $f_{\text{st}}$  if there is some non-negligible lepton asymmetry (Shi & Fuller 1999) or if some other production channels contributed more than the oscillations to the sterile neutrino relic abundance (Kusenko 2009).

LKB did not detect a sterile neutrino emission line in Ursa Minor *Suzaku* spectra. The line flux upper limit was used to derive an excluded region in the  $m_{\text{st}} - \theta$  plane for the case where all of the dark matter is composed of sterile neutrinos. A more general constraint was inferred from the condition that the line flux upper limit not be overproduced through oscillations at the sterile neutrino relic density corresponding to each pair  $(m_{\text{st}}, \theta)$ . We derived line flux upper limits using a maximum-likelihood approach that, along with the lack of intrinsic X-ray emission, enabled us to minimize systematics, and account for those that remained. The resulting constraints on sterile neutrinos are illustrated in Figure 9 of LKB. Although the constraints from this single *Suzaku* observation are comparable to previous results over the entire 1–20 keV mass, the allowed range does not rule out sterile neutrinos as a viable dark matter candidate. We therefore expanded our search to the Willman 1 system – conducting the first X-ray observation of one of the new SDSS dwarf spheroidal galaxies. The capabilities of the *Chandra* X-Ray Observatory are well-suited to the compact size of Willman 1; and, these data provide a good complement to the broader beam observations of the more extended classical Milky Way dwarf spheroidals (Section 4.2).

## 2. Data Analysis

### 2.1. Observation and Data Processing

Willman 1 (*Chandra* ObsID 10534, SeqNum 600727) was observed by *Chandra* on January 27–28 2009 for 102745.5 seconds. The data was taken in TIMED VFaint mode, and was pipeline-processed on 2009-2-10 using `ascdsver 7.6.11.10`. We use CIAO version 4.1.2 (CALDB 4.1.4), and XSPEC version 12.5 in our analysis. Chips 0, 1, 2, 3, 6, 7 were on during the observation. Willman 1 was positioned at the ACIS-I aimpoint, and we generally restrict our analysis to the I-array (chips 0–3) data.

We analyze the standard level 2 event file, and also reprocess the level 1 event file in order to implement the VFaint data-mode quiescent background reduction technique.<sup>1</sup> For the latter, likely background events are flagged based on the pulse heights in border pixels of

---

<sup>1</sup><http://cxc.harvard.edu/ciao/threads/aciscleanvf>

the 5x5 pixel event islands; default split threshold and trail parameters are adopted. These events, as well as those corresponding to bad grades, are removed as the new level 2 event file is generated. No flares are found upon examination of the light curves; and, time intervals where the count rate deviates by more than 10% of the mean are excised. The final exposure times are 99400 and 97100 seconds for the cleaned pipeline processed and reprocessed event files, respectively.

## 2.2. The Background

We consider off-axis (S2, *i.e.* chip 6), blank sky, and stowed data sets as candidates for constructing background spectra. The last corresponds to events collected with the ACIS stowed while the HRC-I is in the focal plane; and, has been demonstrated to be consistent with the dark moon.<sup>2</sup> That is, it can provide an estimate of the pure particle background (PB). In contrast, the blank sky and S2 data include the cosmic (CXB) and galactic (GXB) X-ray backgrounds (which vary over the sky, especially the GXB). The blank sky and stowed event files are reprojected using the Willman 1 aspect solution. The quiescent PB reduction procedure may also be applied to these background event files. If dark matter is composed of sterile neutrinos, their presence in the Milky Way results in line emission in the S2 and blank sky data that will reduce the signal if subtracted out as background. Additionally, the S2 chip is still within the solid angle subtended by the Willman 1 dark halo (see below). Therefore, our constraints are derived from the PB-subtracted spectra from which no astrophysical sources of extended X-ray emission have been eliminated.

## 2.3. Spectral Analysis Setup

Source and background spectra are extracted from identical 5' circular apertures centered on the Willman 1 position or its equivalent in detector coordinates, except for the S2 chip background spectrum that is extracted from a 3' circle optimized in a way that accounts for chip uniformity and point sources near the edge of the chip. The S2 chip center is 15' (165 pc) from the position of Willman 1, and lies outside the region where stellar velocities are measured. The allowed dark matter profile thus spans a large range: the average surface mass density in this field may be as large as  $\sim 50\%$ , or as small as  $\sim 10\%$ , that in the central I-array extraction region. Regions corresponding to point sources detected in the Willman 1 image via application of the CIAO wavelet point source detection algorithm are excluded.

---

<sup>2</sup><http://cxc.harvard.edu/contrib/maxim/stowed/>

Background spectra are re-scaled based on the relative count rates in the 9-12 keV band where virtually all events are due to the PB. The PB has been found to vary significantly in normalization, but not in shape, so that the rescaled PB spectra can be used to construct an appropriate PB-subtracted source spectrum.<sup>3</sup>

## 2.4. Spectral Analysis

In our analysis of the *Suzaku* data on the Ursa Minor dwarf spheroidal galaxy, we based our constraints on the total (unsubtracted) spectrum. Because the *Chandra* PB is higher, but more precisely determined, we adopt a more conventional approach here and consider background-subtracted spectra, grouped to a minimum of 15 counts per bin, utilizing  $\chi^2$  statistics to derive best fits and parameter uncertainties.

The cleanest PB subtraction is realized utilizing the source and stowed background spectra with application of the VFaint data-mode quiescent background reduction technique, although using the corresponding pipeline-processed datasets yielded similar results (with slightly larger uncertainties). The source spectrum is fitted with a model consisting of a solar abundance thermal plasma (to model the GXB) and power-law (to model the CXB) absorbed by the Galactic column density. In this case the GXB component is not required, although the upper limit on the flux is consistent with the larger-scale average GXB surface brightness measured in the *ROSAT All-Sky Survey*. The best-fit ( $\chi^2/\nu = 1.09$ ) power-law photon index is 1.8 (1.4-2.7 at 90% confidence), and the normalization consistent with the fraction of the CXB unresolved by our observation ( $\sim 25\%$ ; Mushotzky et al. 2000). Figures 1a and 1b show the total, (stowed) background, and background-subtracted spectra for cases utilizing pipeline-processed, and reprocessed (reduced-background) event lists. The best-fit power-law model, and fit residuals, are also shown. We show the full 0.3-12 keV energy band, although the fits are conducted over 0.4-7 keV. There are PB-related residuals in the background-subtracted spectrum above 7 keV where the *Chandra* sensitivity experiences a steep decline. Some of these persistent residuals may be attributed to the fact that the time-dependent gain correction cannot be re-applied to the background data, as was done with the source data.

The blank-sky background (SB) is significantly brighter than the source spectrum below 1 keV. The total PB-subtracted 0.4-7 keV surface brightness is  $\approx 1.7\times$  higher in the SB than in Willman 1. Evidently the GXB is brighter in the former and, as a result, the SB-subtracted spectrum ought to be utilized with care (Figure 2). Also, as previously mentioned, if there is

---

<sup>3</sup><http://cxc.harvard.edu/contrib/maxim/bg/>

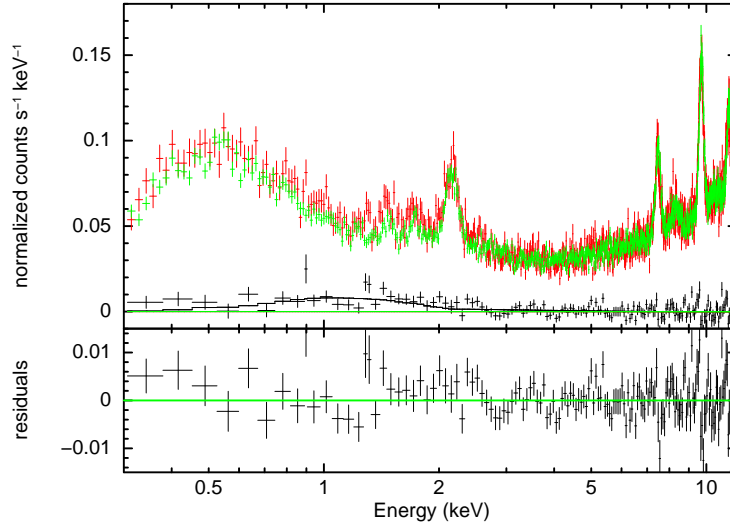
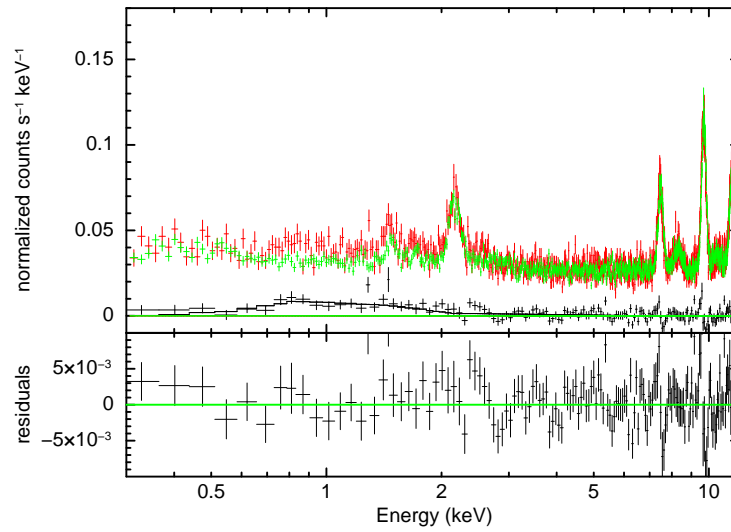


Fig. 1.— **(a) top:** Total (red), PB (green), and source (*i.e.* PB-subtracted; black) spectra. The histogram is the best-fit GXB+CXB model to the source spectrum. **(b) bottom:** Same as **top** with the quiescent-particle-background reduced in the total and PB spectra as explained in the text.



dark matter decay in the X-ray band there will be a contribution from the Milky Way halo to the SB that is absent in the PB.

### 3. Limits on Sterile Neutrino Parameters from the *Chandra* Spectrum of Willman 1

In deriving upper limits, we divide the spectrum into low ( $< 1.1$  keV) and high ( $> 1.1$  keV) energy segments, since any GXB emission will be negligible in the latter. The high energy segment best-fit ( $\chi^2/\nu = 1.11$ ) power-law slope is 1.77 (1.22-2.37 at 90%, confidence). At low energies, power-law ( $\chi^2/\nu = 0.95$ , slope =  $2.27_{+1.39}^{-1.09}$ ) and thermal **apec** ( $\chi^2/\nu = 0.92$ ,  $kT = 0.48 \pm 0.15$  keV) models provide acceptable fits. We conduct Monte Carlo numerical experiments (LKB, and references therein) where we find that, in fits to simulated continua spectra with models that include an emission line, the fit is improved by  $\Delta\chi^2 = 9.2$  with  $\sim 1\%$  frequency – closely approximating that for a  $\chi^2$  distribution with two degrees of freedom. We thus adopt  $\Delta\chi^2 = 9.2$  flux limits, derived from adding an unresolved Gaussian component in 10 eV intervals over the 0.4-7 keV bandpass to simulated spectra of the best-fit line-free model. The errors are averages over 100 simulations that are initiated using parameters from fits to a seed simulation (and not the best-fit parameters to the actual data), so that the uncertainties in the parameter values are taken into account. Line fluxes are allowed to go negative (as is the case with the simulations). The upper and lower line flux limits, in 200 eV bins, based on the PB-subtracted fits are shown in Figure 3. The latter are negative over the entire 0.4-7 keV bandpass. The constraints based on the SB-subtracted fits are similar in magnitude above 2 keV.

The mapping of the Willman 1 constraints onto the sterile-neutrino-mass-mixing-angle plane (equation 4) is shown in Figure 4a. As discussed above (Section 1.3; see also Section 3 in LKB and Section 5 below) there are two kinds of limits, both of which are shown. The first assumes only that the thermal history of the universe is given by standard Big Bang cosmology. Sterile neutrinos are ruled out for the region in parameter space where the flux from sterile neutrinos produced at minimal abundance via the DW mechanism (Asaka, Laine, & Shaposhnikov 2007) exceeds our derived limits. The second limit is that which overpredicts the derived limits if sterile neutrinos account for 100% of the dark matter (dark-matter fraction of sterile neutrinos  $f_{\text{st}} = 1$ ), regardless of how they are produced. In Figure 4b, the former limits, which are the most general, are compared with those we derived in Ursa Minor with *Suzaku*.

The smaller *Chandra* beam and more compact Willman 1 dark matter distribution compensate somewhat for the higher sensitivity of the *Suzaku* measurement to yield constraints

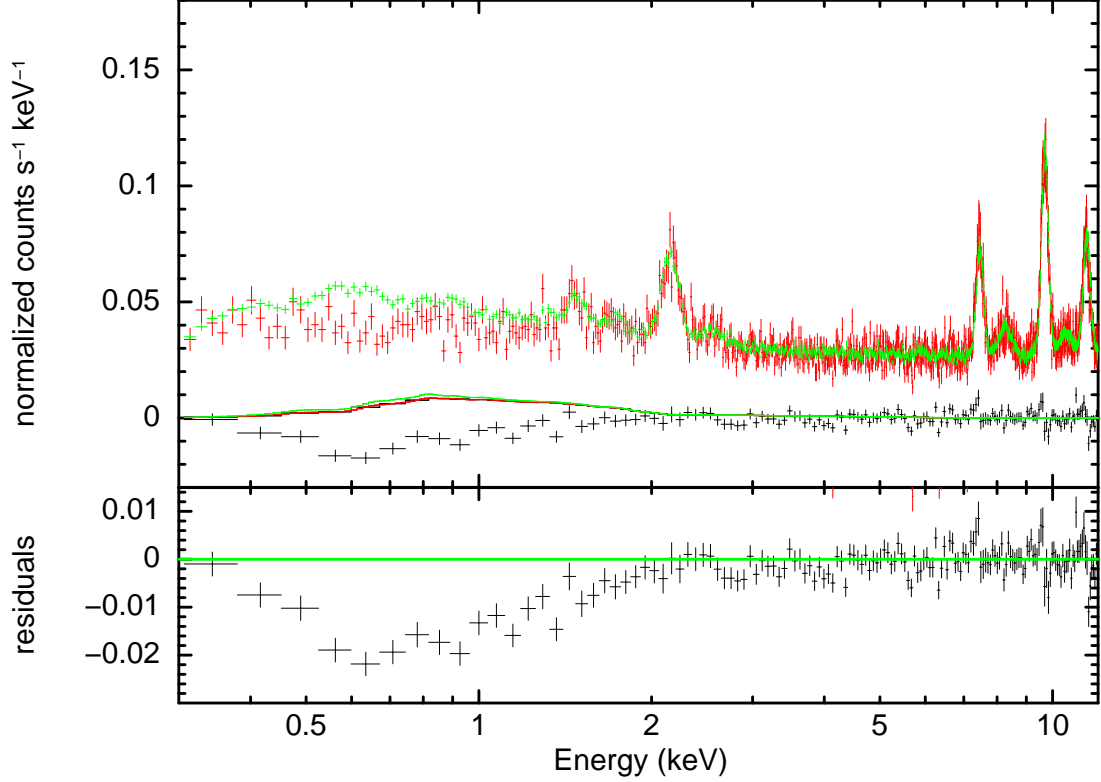


Fig. 2.— Total (red), SB (green), and SB-subtracted (black) spectra. The histogram is the best-fit GXB+CXB model to the *PB-subtracted* spectrum of Figure 1b. The SB results in an oversubtraction below 2 keV. Due to the contribution of the Milky Way halo the SB is expected to contain the dark-matter signal as well; and, therefore subtraction of the SB can simultaneously lower both the background and the signal. The oversubtraction below 2 keV and the weakening of the signal due to subtraction of the Milky Way contribution are the two reasons why we do not use the SB-subtracted spectrum for data analysis.

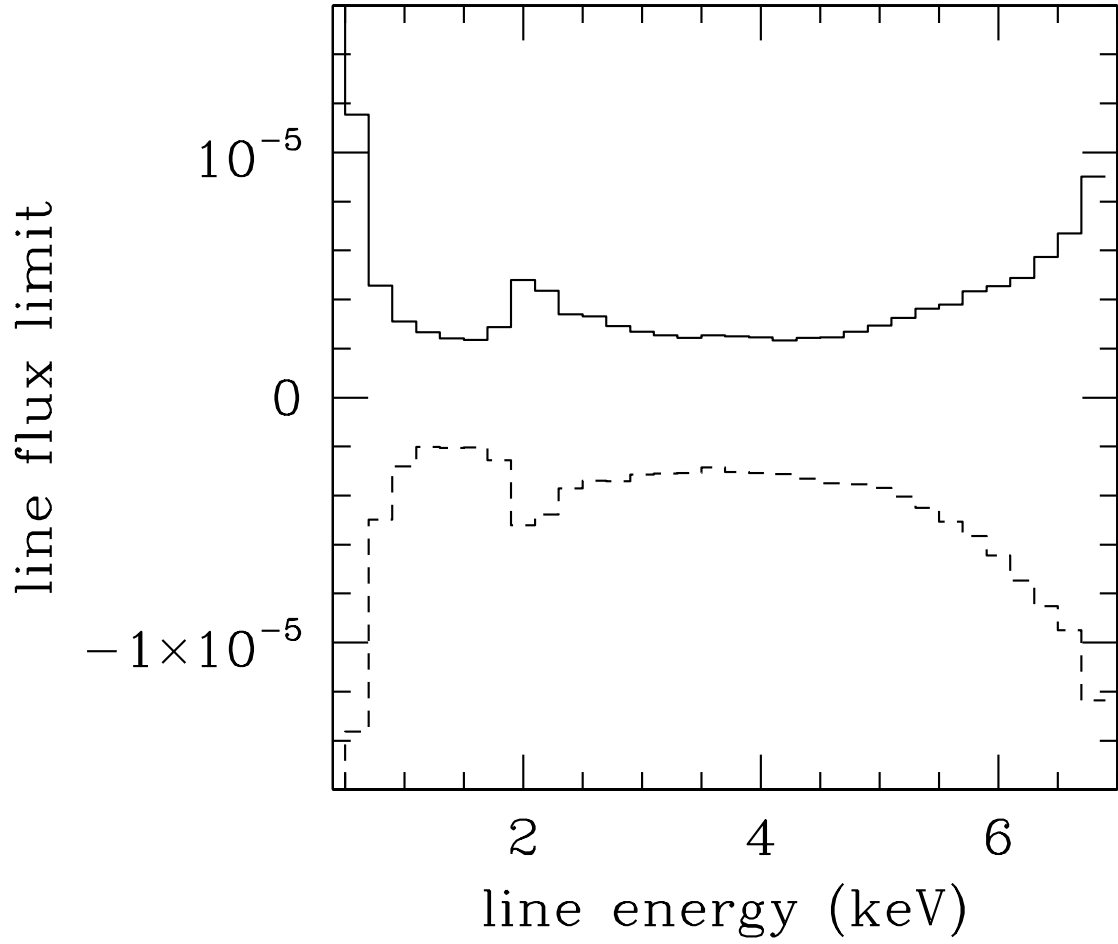


Fig. 3.—  $\Delta\chi^2 = 9.2$  line flux upper (solid histogram) and lower (broken histogram) limits in photons  $\text{cm}^{-2} \text{s}^{-1}$ .

at sterile neutrino masses  $< 14$  keV (corresponding to photon energies in the spectra  $< 7$  keV) of similar magnitude to those derived for Ursa Minor in LKB. This comparison utilizes a projected mass enclosed within the relevant radius of 55 pc ( $5'$  at 38 kpc)  $M_{\text{pro}} = 2 \times 10^6 M_{\odot}$  – corresponding to a mass surface density of  $\Sigma = 210 M_{\odot}\text{pc}^{-2}$  – as determined by projecting the best-fit NFW (Navarro, Frenk, & White 1997) mass model in Strigari et al. (2008b). The 90% confidence contours for the NFW parameters allow values of  $M_{\text{pro}}$  that are  $4\times$  lower, and  $2 - 3\times$  higher. In addition, we estimate that the Milky Way dark matter halo and the extragalactic dark matter contribute an additional  $65 - 125 M_{\odot}\text{pc}^{-2}$  (Xue et al. 2008, and references therein). While maintaining a fiducial mass of  $2 \times 10^6 M_{\odot}$ , we show the effect on the general constraints of varying the surface density, and hence the effective mass in the FOV, by factor of two in either direction in Figure 4b.

#### 4. A Candidate Line at 2.5 keV

In addition to the limits derived above, we present evidence of a spectral feature consistent with a 2.5 keV line from decay of a 5 keV relic sterile neutrino.

##### 4.1. Line Flux and Statistical Significance

The largest residual excess emission to the PB-subtracted Willman 1 spectrum with respect to the best-fit continuum model occurs at  $\sim 2.5$  keV. When we add an additional Gaussian component, we find that  $\chi^2$  improves by 5 (Figures 5 and 6). The line-width is consistent with an unresolved feature broadened only by the instrumental line spread function, as expected considering the small Willman 1 velocity dispersion. For power-law-plus-Gaussian fits to the 2.2-5 keV spectrum, the best-fits and uncertainties on the line energy and flux are  $2.51 \pm 0.07(0.11)$  keV and  $[3.53 \pm 1.95(2.77)] \times 10^{-6}$  photons  $\text{cm}^{-2} \text{s}^{-1}$ , where the errors are 68% (90%) confidence limits for two degrees of freedom corresponding to  $\Delta\chi^2 = 2.3$  (4.61) (Section 3; Yaqoob 1998). The corresponding confidence contours are shown in Figure 7, as is the  $\Delta\chi^2 = 9.21$  (99% confidence) contour. The 2.2 keV limit was chosen to avoid the energy associated of the peak of the brightest of the PB Au fluorescence lines, and with the deep *Chandra* mirror iridium edge (Chartas et al. 2000; there is also a shallow edge at  $\sim 2.55$  keV that does not impact our results). The issue of these instrumental features is specifically addressed in Section 4.2.4. However, extending the range to the full 1.1-7 keV high energy segment bandpass yields a consistent measurement ( $F_{\text{line}} = [2.85 \pm 1.85(2.57)] \times 10^{-6}$  photons  $\text{cm}^{-2} \text{s}^{-1}$ ) as do fits over other subsets of this bandpass. In the 2.4-2.6 keV energy interval, the total, PB, and source counts are  $696 \pm 26.4$ ,  $601 \pm 13.6$ , and

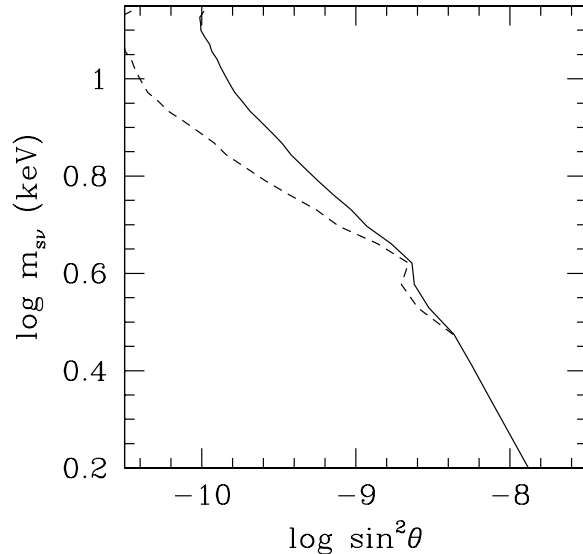
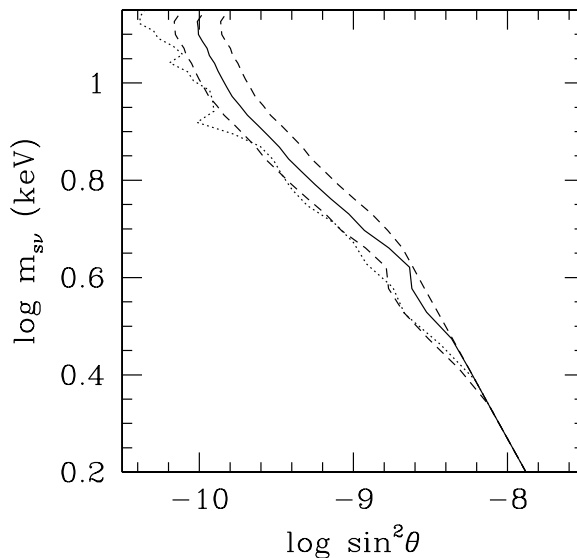


Fig. 4.— **(a) top:** The sterile neutrino parameter space to the right of the solid curve is excluded by the *Chandra* observation of Willman 1 assuming only that DW production by neutrino oscillations takes place. The sterile neutrino parameter space to the right of the broken curve is excluded if 100% of dark matter is composed of sterile neutrinos produced by some (unspecified) mechanism. The mass of  $2 \times 10^6 M_\odot$  is derived from the best-fit NFW (Navarro, Frenk, & White 1997) mass model in Strigari et al. (2008b). **(b) bottom:** The solid curve from (a) is reproduced and compared to constraints assuming projected masses of 1 and  $4 \times 10^6 M_\odot$  (broken curves; see text), and to the constraints derived from *Suzaku* observation of Ursa Minor (dotted line).



$95 \pm 30$ , respectively. In the composite models the emission line component accounts for 90% of the flux. 20 counts in this interval are expected based on the best-fit power-law model *without a line*. Figure 8 shows the unfolded spectrum – the ratio of the data values to the product of the model multiplied by the response, all multiplied by the model values – over the 1.5-5 keV spectral region.

The feature is not positively detected in the global blank sky spectrum (Abazajian et al. 2007, and references therein). The  $\Delta\chi^2 = 4.61$  upper limit based on the reprojected estimated SB of Willman 1 is  $2.1 \times 10^{-6}$  photons  $\text{cm}^{-2} \text{s}^{-1}$ . When we utilize the SB, or appropriately-scaled S2, spectrum as background the fits are not significantly improved in models with an additional emission line, although the upper limits are consistent with the line flux based on the PB-subtracted spectrum. As the SB (Figure 2) and S2 spectra overestimate the Willman 1 background, and will include a contribution due to the Milky Way dark matter halo (plus, possibly significant, additional emission from the outer Willman 1 halo in the latter), the expectation that the PB-subtracted spectrum is most sensitive for these purposes is confirmed.

Notably, the flux is consistent with the narrow region in the mass-mixing-angle plane where the DW neutrino oscillation mechanism produces all of the dark matter (and where sterile neutrino emission from neutron stars may explain pulsar kicks – see next section). Figure 9 shows the predicted flux at each energy  $E_\gamma$  assuming DW production of sterile neutrinos of  $m_{\text{st}} = 2E_\gamma$ , and  $f_{\text{st}} = 1$ . We compare this with the  $\Delta\chi^2 = 4.61$  upper limits derived from Monte Carlo simulations (see Section 3), and our measurement. Even accounting for uncertainties in the DW production rate, and allowing for a factor of four uncertainty in the mass, a fluctuation at this level maps into this narrow region only over  $\sim 1 - 3.5$  keV. At lower energies the predicted line flux is below our sensitivity, while at higher energies a much stronger feature would be expected. That is, the likelihood of a marginal feature compatible with the simplest sterile neutrino hypothesis is much less than the likelihood at some random X-ray energy.

## 4.2. Discussion

### 4.2.1. Comparison with Limits from Classical Milky Way Dwarf Spheroidals

We re-examine the *Suzaku* spectra of the Ursa Minor and Draco “classical” Milky Way dwarf spheroidals to check for consistency with the line flux limits of the 2.5 keV candidate sterile neutrino radiative decay emission line in Willman 1. The projected mass estimate adopted in LKB within the *Suzaku* spectral source region for Ursa Minor is  $\sim 30\times$  our

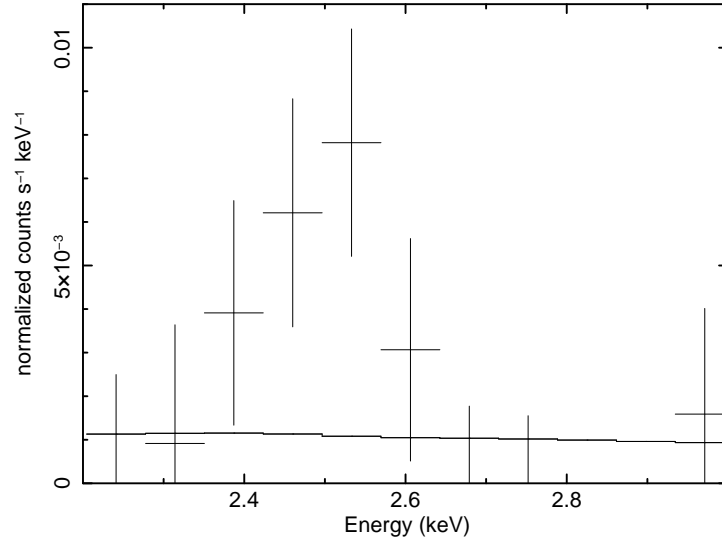
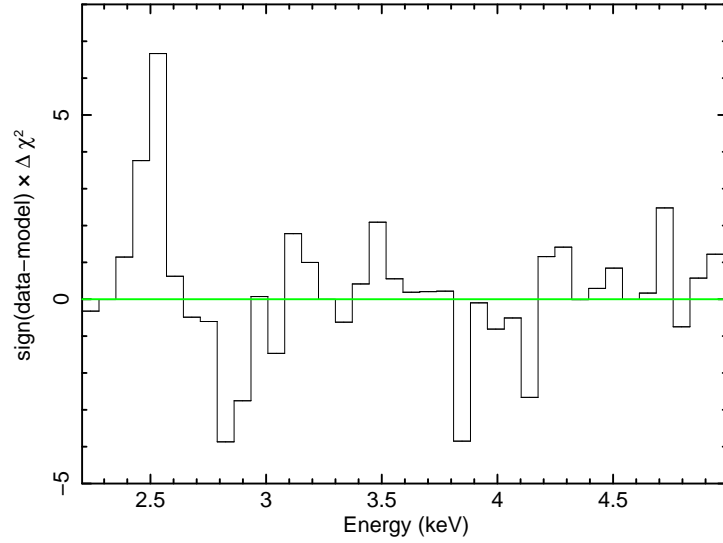


Fig. 5.— **(a)** Data and best-fit power-law model to the 2.2-5 keV spectrum, in the 2.2-3 keV energy region **(top)**, and **(b)** contributions to  $\chi^2$  over 2.2-5 keV **(bottom)**.



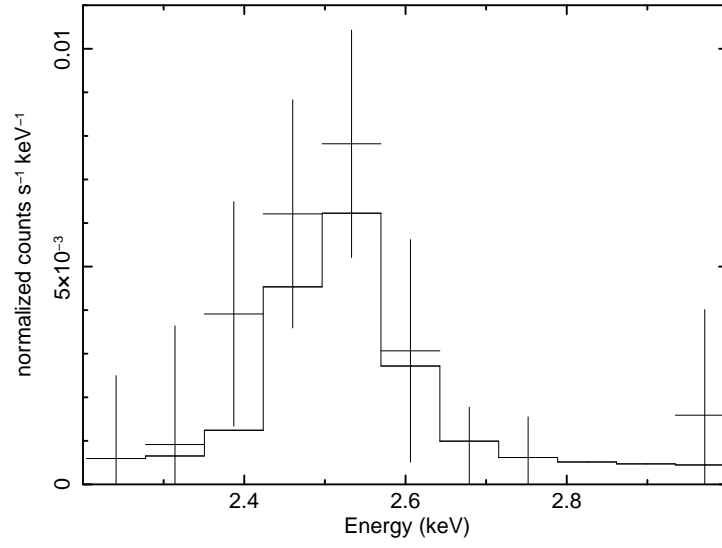
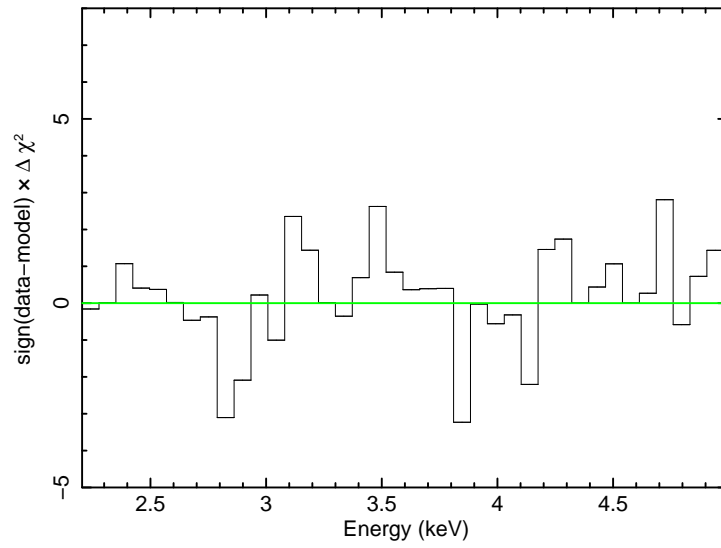


Fig. 6.— Same as Figure 5 for the best-fit power-law-plus-Gaussian model.



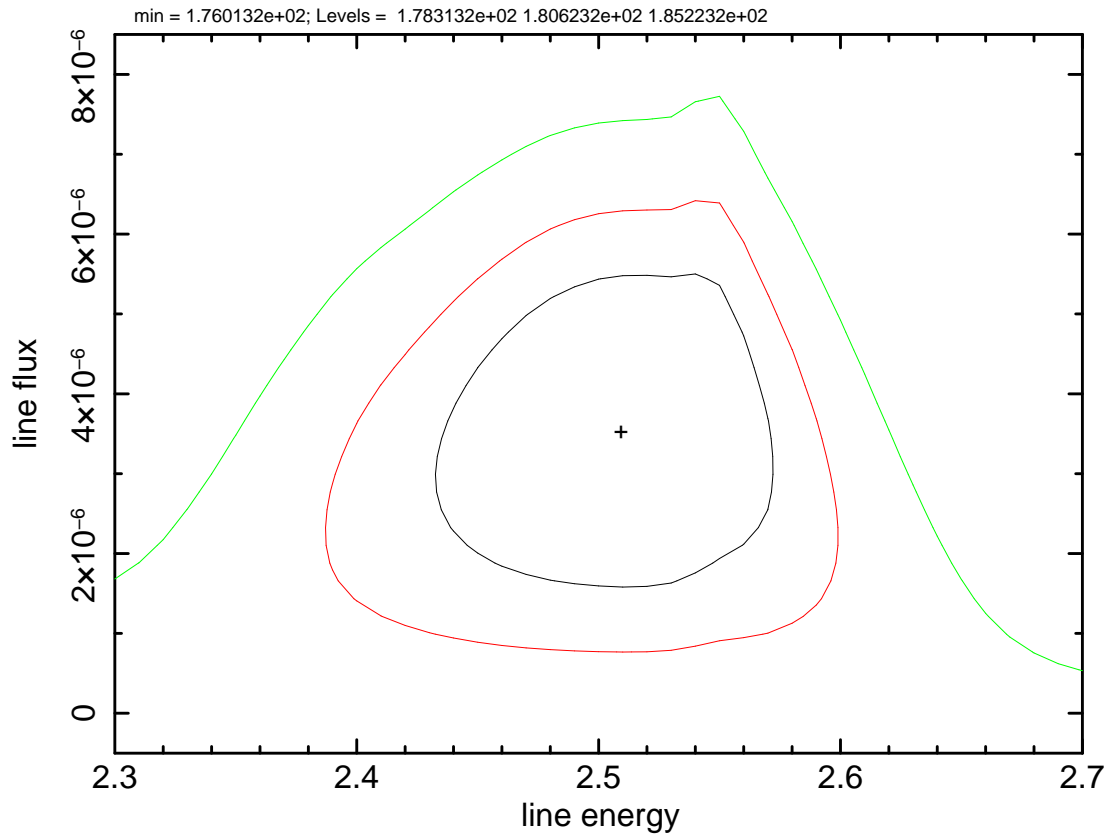


Fig. 7.—  $\Delta\chi^2 = 2.3, 4.61,$  and  $9.21$  confidence contours for the emission line parameters.

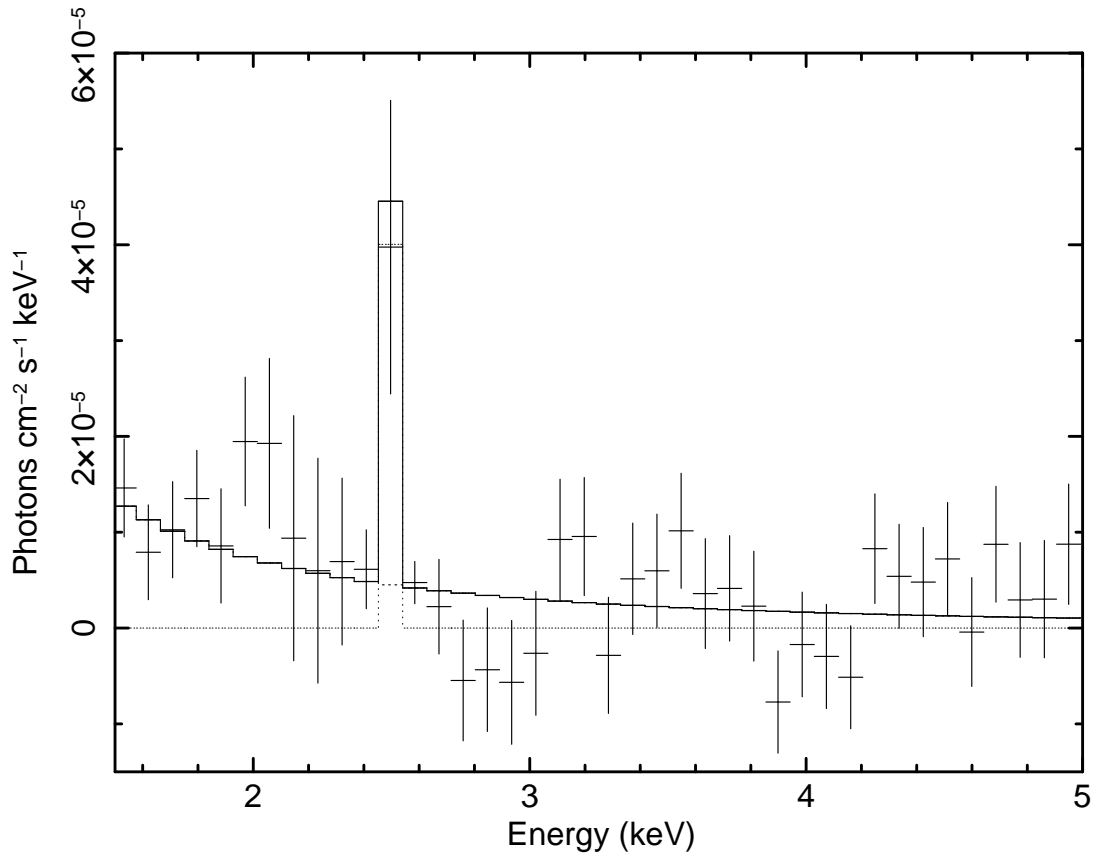


Fig. 8.— Unfolded 1.5-5 keV spectrum; see text for details.

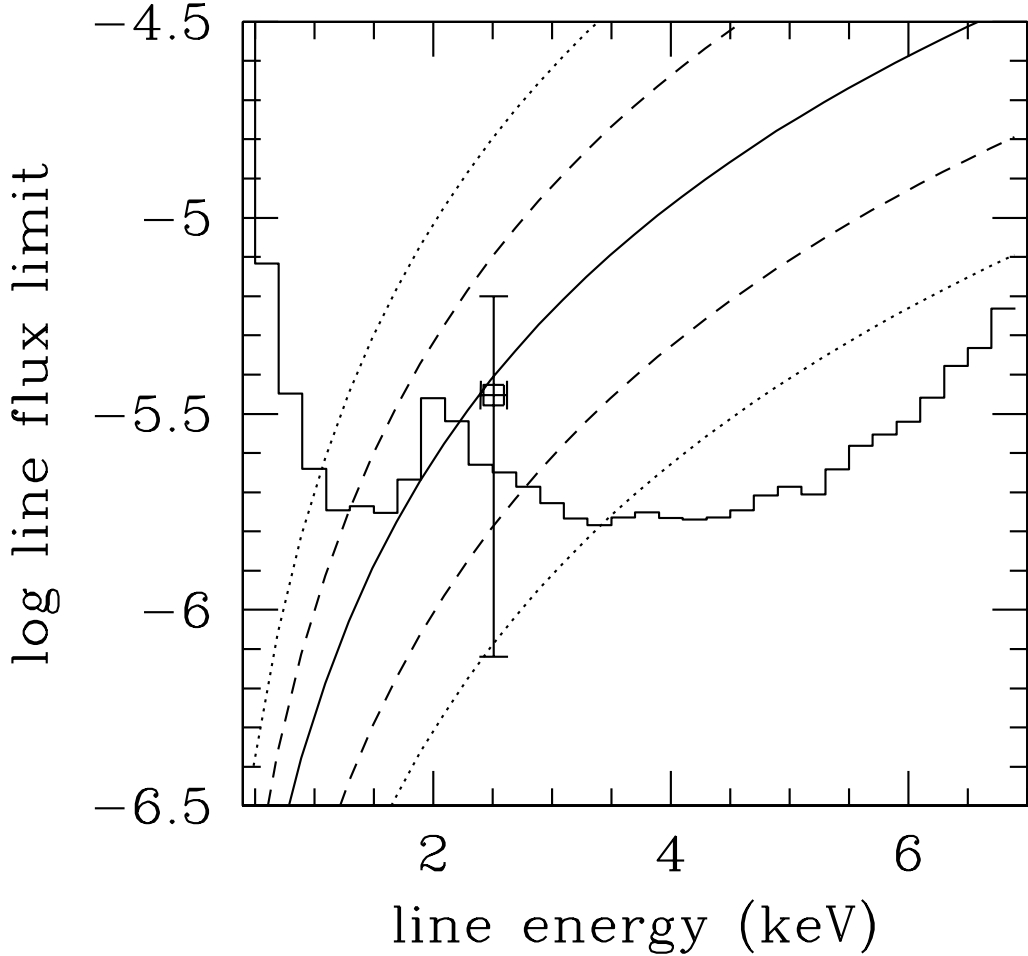


Fig. 9.— The histogram shows the  $\Delta\chi^2 = 4.61$  upper limits for a line-free spectrum. The solid and broken lines show the expected line flux from sterile neutrino radiative decay in Willman 1, assuming  $f_{\text{st}} = 1$  and taking into account the hadronic uncertainties in production (Asaka et al. 2007), which affect the relation between the mass and the mixing angle corresponding to a given value of  $f_{\text{st}}$ . The dotted curves allows for a factor of two uncertainty in mass in either direction ( $M_7 = 0.1 - 0.4$ ), *in addition* to the spread in possible production rate.

fiducial value for the mass within the (smaller) Willman 1 *Chandra* extraction region. Draco has a similar projected mass to that of Ursa Minor (Strigari et al. 2007a).

Factoring in these mass ratios, and their respective distances, the 90% limits of the Willman 1 line flux translates to a predicted flux of  $(3.2 \pm 2.5) \times 10^{-5}$  photons  $\text{cm}^{-2} \text{s}^{-1}$  in Ursa Minor. In re-analyzing these spectra, we focus on the 1.3-5.2 keV energy region and, as in LKB, fit the *unsubtracted* and unbinned spectrum to a model that includes power-law and Gaussian non-X-ray background (PB) components (see LKB for details on how the spectra are segmented, and other details). An additional line is not required based upon simultaneous re-analysis of the *Suzaku* XIS1 (frontside-illuminated) and XIS03 (co-added backside illuminated) spectra – in fits where the line flux is tied in the two spectra. However, fits to the XIS1 spectra, when analyzed independently, are improved by the addition of such a line ( $\Delta C=7$ , where C is the Cash-statistic; Cash 1979). The best fit line energy is 2.41 keV with 90% confidence limits 2.35-2.57 keV (and a secondary local minimum at  $\sim 2.5$  keV); the line flux is  $(2.5 \pm 1.9) \times 10^{-5}$  photons  $\text{cm}^{-2} \text{s}^{-1}$  (Figure 10a) – consistent with the expectations. However, the line is not detected in the (less sensitive) XIS03 Ursa Minor spectrum: the upper limit is  $1.8 \times 10^{-5}$  photons  $\text{cm}^{-2} \text{s}^{-1}$  (Figure 10b). The *Suzaku* spectra of Draco, reduced and analyzed in an identical manner, do not require a 2.5 keV line. The upper limit from simultaneous fits is  $\sim 2.5 \times 10^{-5}$  photons  $\text{cm}^{-2} \text{s}^{-1}$ , with similar limits from the individual detectors. Because of its larger distance, the expected flux from Draco is  $\sim 25\%$  smaller than for Ursa Minor.

Riemer-Sorensen & Hansen (2009) analyzed archival data (ObsIDs 9589 and 9776) of the Draco dwarf spheroidal galaxy. We have re-analyzed these data, essentially replicating their reduction procedures, but deriving line flux upper limits from the spectrum extracted from a 4' circular aperture by application of the procedure used to derive limits for Willman 1 (Section 3). There are significant differences in the two datasets. The Willman 1 observation is about three times deeper; and was centered on the I-array instead of the S3 chip. The latter has  $\sim 30\%$  higher effective area at 2.5 keV,<sup>4</sup> but also a higher background. Other factors that contribute to a lower background in the Willman 1 observation are the lower point source detection threshold (about 5 times as many point sources are detected), the higher concentration of Willman 1 that allows us to use a smaller spectral extraction region, and the ability to pre-filter the particle background (see section 2; the Draco observation was conducted in FAINT, rather than VFAINT, data-mode). We derive a 90% upper limit at  $\sim 2.5$  keV of  $2.0 \times 10^{-6}$  photons  $\text{cm}^{-2} \text{s}^{-1}$  in Draco, consistent with the results of Riemer-Sorensen & Hansen (2009). Based on an estimated projected mass of  $\sim 6 \times 10^6$

---

<sup>4</sup><http://exc.harvard.edu/proposer/POG/>

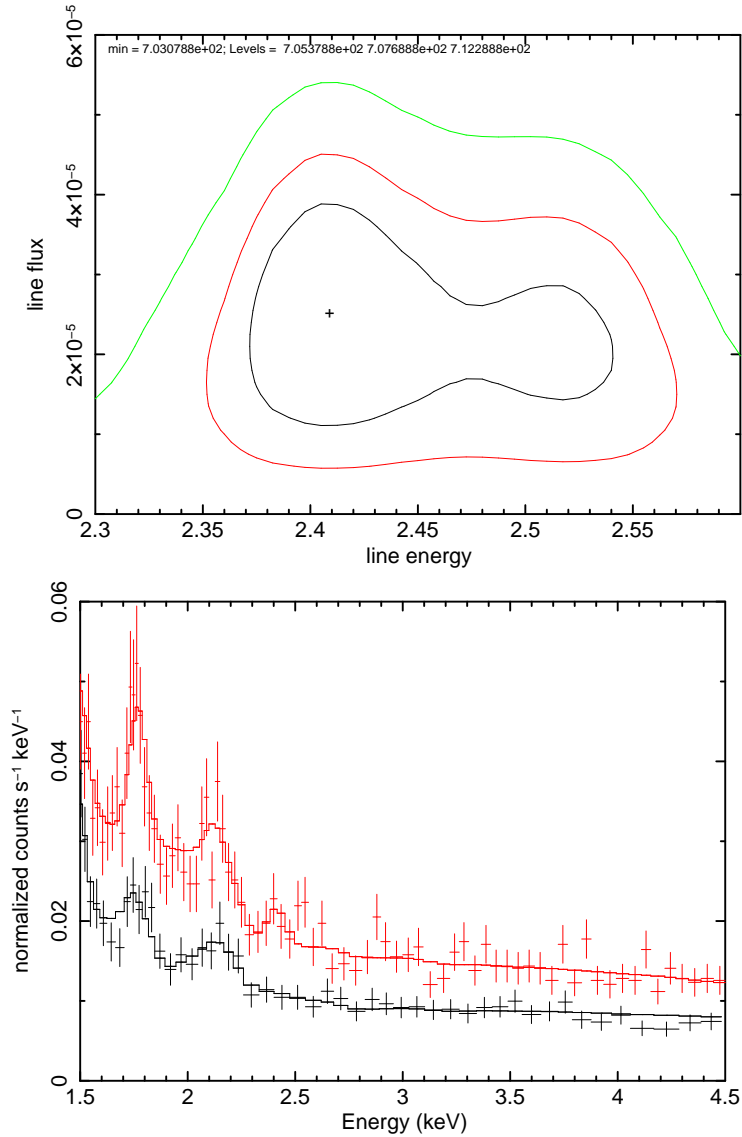


Fig. 10.— **(a) top:**  $\Delta C = 2.3, 4.61,$  and  $9.21$  confidence contours for the emission line parameters, from the *Suzaku* XIS1 spectrum of Ursa Minor. **(b) bottom:** XIS1 (red) and XIS03 (black) spectra and best fit models that include a  $\sim 2.4$  keV line (the flux is  $2.5 \times 10^{-5}$  photons  $\text{cm}^{-2} \text{s}^{-1}$  in the former, and 0 in the latter).

$M_{\odot}$  (Strigari et al. 2007a), the expected flux is  $\sim 75\%$  that in Willman 1 (Draco is twice as distant) – *i.e.*  $(2.5 \pm 2) \times 10^{-6}$  photons  $\text{cm}^{-2} \text{s}^{-1}$ .

#### 4.2.2. Other Dark Matter Dominated Systems

Some of the strongest claimed limits on sterile neutrino parameters are derived from M31 (Watson et al. 2006; Boyarsky et al. 2008, 2010). These depend on estimates of the dark matter content in regions where baryonic matter is significant, if not dominant. While there is a fairly strong consensus on the total mass in M31, there is a wide range of possible mass decompositions (primarily) into stellar disk, stellar bulge, and dark matter halo components (Chemin, Carignan, & Foster 2009; Corbelli et al. 2009; Saglia et al. 2010) – wider than assumed in the papers referred to above. The best-fits presented in Corbelli et al. (2009) are obtained using the Burkert (1995) dark matter density distribution function. The resulting projected dark matter mass of  $2.9 \times 10^9 M_{\odot}$  (for models with constrained virial mass) in the 1.1-3 kpc annulus, demonstrates that a non-detection in M31 does not stand in contradiction to a feature in Willman 1 with best-fit parameters we derive from the *Chandra* data (Kusenko and Loewenstein 2010).

The diluting effects of X-ray emission associated with stellar and/or hot plasma presents a potential complication in systems with prominent baryonic components. For galaxies, we estimate the contribution from an old stellar population of mass  $M_*$  to the luminosity emitted in an energy interval  $\Delta E$  at 2.5 keV, using the power-law indices and normalizations in Revnivtsev et al. (2008), as

$$L_{\Delta E}(2.5\text{keV})/M_* = 1.0 \times 10^{26} [1 + 40(1 - f_{\text{res}})] \frac{20\Delta E}{E}, \quad (5)$$

where the ratio  $\Delta E/E$  is normalized to a typical CCD spectral resolution (at 2.5 keV) of 20. The first term accounts for cataclysmic variable and coronally active binary stars, as seen in the Milky Way and M31 (Li & Wang 2007; Bogdan & Gilfanov 2008). The second accounts for low mass X-ray binaries, with  $f_{\text{res}}$  the fraction of the LMXB flux that is resolved out (which depends on the angular resolution and exposure depth of the observation, as well as the LMXB luminosity function). The ratio of this term to the sterile neutrino radiative decay line emission from the dark matter mass  $M_{\text{dark}}$  is

$$[0.111 + 4.44(1 - f_{\text{res}})] \frac{20\Delta E}{E} \Gamma_{-27}^{-1} \frac{M_*}{M_{\text{dark}}}. \quad (6)$$

This emission, that may be augmented by discrete sources and hot gas associated with a more recent star formation, may be non-negligible where dark matter is subdominant or marginally dominant.

In galaxy clusters and groups, and massive elliptical galaxies, that are filled with hot ( $\sim 1 - 10$  keV) plasma enriched with the products of star formation, emission of a 2.5 keV sterile neutrino decay line may be overwhelmed by  $K\alpha$  emission lines at  $\sim 2.45$  and  $\sim 2.6$  keV from He-like and H-like S, respectively. For example, in M87 the observed S XV line flux (Matsumoto et al. 1996) within  $10'$  is  $\sim 10\times$  that expected from the amount of dark matter (Churazov et al. 2008) if it were composed of sterile neutrinos decaying at the rate inferred in Willman 1.

Of course, the gravitational potential wells in dwarf spheroidals are far too shallow (their observed velocity dispersions corresponding to  $\sim 10$  eV temperatures) to bind gas hot enough to collisionally ionize S to this degree, and there are no significant sources of photoionization. If hot plasma were somehow responsible for the Willman 1 2.5 keV emission line, one would expect much stronger accompanying emission in Si-K and Fe-L shell emission that is not seen – unless the elemental abundances are highly and uniquely peculiar. When we attempt to fit the Willman 1 spectrum with a thermal plasma model (best fit temperature,  $kT \sim 2$  keV), we find that the 2.5 keV line may be accounted for only if the S/Fe abundance ratio exceeds  $50\times$  the solar ratio.

#### 4.2.3. Other Constraints

The limits based on Lyman- $\alpha$  forest data (Boyarisky et al. 2009) allow up to 40% of dark matter in the form of 5-keV sterile neutrinos produced via Dodelson-Widrow (DW) scenario (Dodelson & Widrow 1994). However, if there is any contribution from the Higgs boson decays, the resulting population of relic sterile neutrinos has about three times smaller free-streaming length than the DW population (Kusenko 2006; Petraki 2008; Petraki & Kusenko 2008; Boyanovsky 2008b). The inclusion of the additional “cold” population of sterile neutrinos weakens or eliminates the Ly- $\alpha$  bounds. Although a detailed numerical analysis of such mixed dark matter has yet to be performed, the approximate analytical results indicate that 5 keV sterile neutrinos can account for 100% of dark matter in this case (Petraki 2008; Boyanovsky 2008a,b).

#### 4.2.4. Instrumental Features in Proximity

Improper subtraction of the PB could conceivably produce artefacts in the subtracted spectrum that may be misinterpreted as a feature. We address this issue, as follows, by applying an analysis procedure to the Willman 1 spectrum along the lines that we implemented

in analyzing the *Suzaku* dwarf spheroidal spectra (see Section 4.2.1, LKB). We consider the full unsubtracted, and unbinned, spectrum in the 2.2-5 keV band. The reduced-background PB spectrum (Section 2.4) is fit by a model consisting of a power-law and two Gaussian emission lines with energies corresponding to the brightest Au fluorescent features (Chartas et al. 2000), and line-widths that are free to vary. The addition of a line at 2.51 keV does not improve the fit, and the  $\Delta C = 2.7$  line flux upper limit is  $6 \times 10^{-7}$  photons  $\text{cm}^{-2} \text{s}^{-1}$ . If we then fit the total (unsubtracted) spectrum with the same baseline model, the addition of a line at 2.51 keV improves the fit by  $\Delta C = 5.8$  and the best-fit line flux of  $3.5_{-2.5}^{+2.1} \times 10^{-6}$  photons  $\text{cm}^{-2} \text{s}^{-1}$  ( $\Delta C = 2.7$  errors) is consistent with the estimate based on the PB-subtracted spectrum. If we allow the line energy to float, we find energy  $2.57 \pm 0.06$  keV and flux  $4.2 \pm 2.5 \times 10^{-6}$  photons  $\text{cm}^{-2} \text{s}^{-1}$  ( $\Delta C = 4.6$  errors), again consistent with the initial estimate. The improvement in fit over the baseline model is  $\Delta C = 10.6$ . If we then go back and refit the PB spectrum with an additional line with energy fixed at 2.57 keV, we find that the  $\Delta C = 2.7$  line flux upper limit is  $1.6 \times 10^{-6}$  photons  $\text{cm}^{-2} \text{s}^{-1}$ , and the inclusion of the line does not improve the fit ( $\Delta C = 1.6$ ). These considerations indicate that the 2.5 keV feature is not an artefact of inaccurate PB subtraction. The unbinned PB and total spectra and best fit models are shown in Figure 11ab; the same comparison with the data rebinned (in the plot only) is shown along with the two best-fit models in Figure 12. Confidence contours are plotted in Figure 13.

#### 4.2.5. Consistency, but not Corroboration

Our re-examination of the other X-ray dwarf spheroidal datasets yields an intriguingly similar weak 2.5 keV feature in the *Suzaku* XIS1 spectrum of Ursa Minor, but fails to confirm the presence of an emission line at the expected strength in *Suzaku* and *Chandra* data on Draco and the *Suzaku* XIS03 spectrum of Ursa Minor. Boyarsky et al. (2010) do not detect a feature in either the Sculptor or Fornax dwarf spheroidals; although, it is notable that these systems have relatively low mass-to-light ratios (Wolf et al. 2009) – increasing the possibility of the presence of the diluting effects of an unresolved stellar component (the former is known to have a population of X-ray binaries; Maccarone et al. 2005) – a factor that is also an issue in M31 (see above). Detection of a 2.5 keV line from sterile neutrinos is impeded in the most massive dark-matter dominated systems, which are well known to retain hot metal-enriched (interstellar, intragroup, or intracluster) gas with line-emission from highly ionized S. Such sources of confusion are absent in the extreme baryon-poor faint and ultra-faint dwarf spheroidals, making them the cleanest targets for confirming or refuting the evidence for 5 keV sterile neutrino dark matter uncovered in Willman 1.

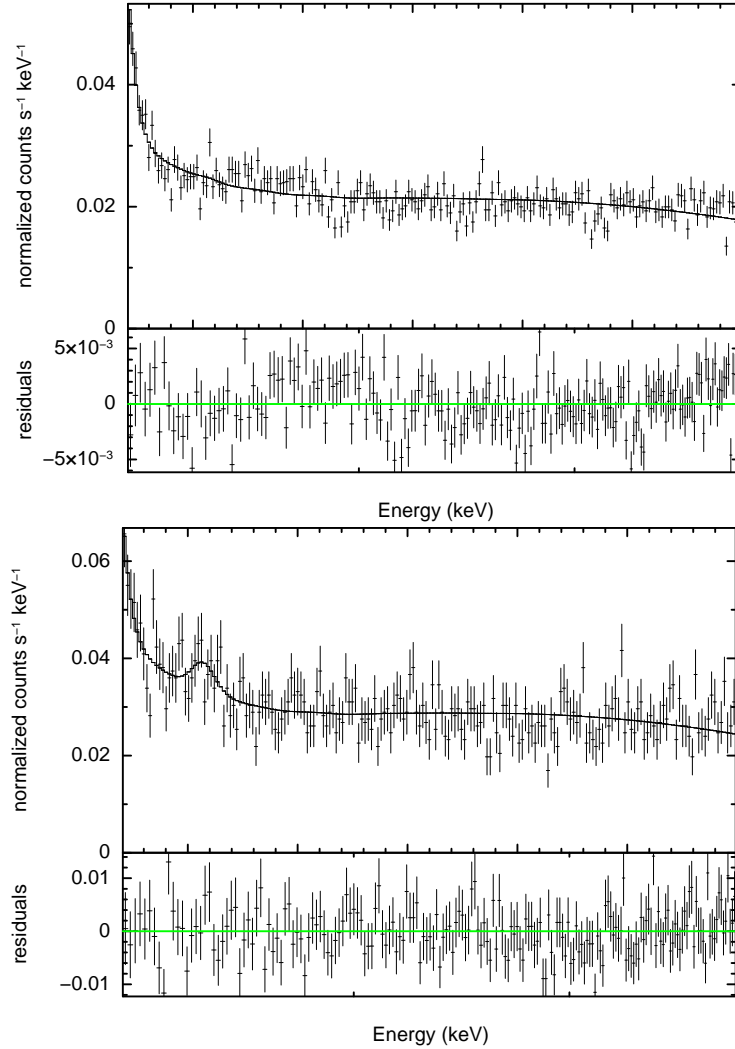


Fig. 11.— **(a) top:** Unbinned PB spectrum and best fit model (see text). **(b) bottom:** Same for total Willman 1 spectrum. Inclusion of an additional emission line, with energy and flux consistent with that obtained from the PB-subtracted data, significantly improves the fit in the total, but not the PB, spectrum.

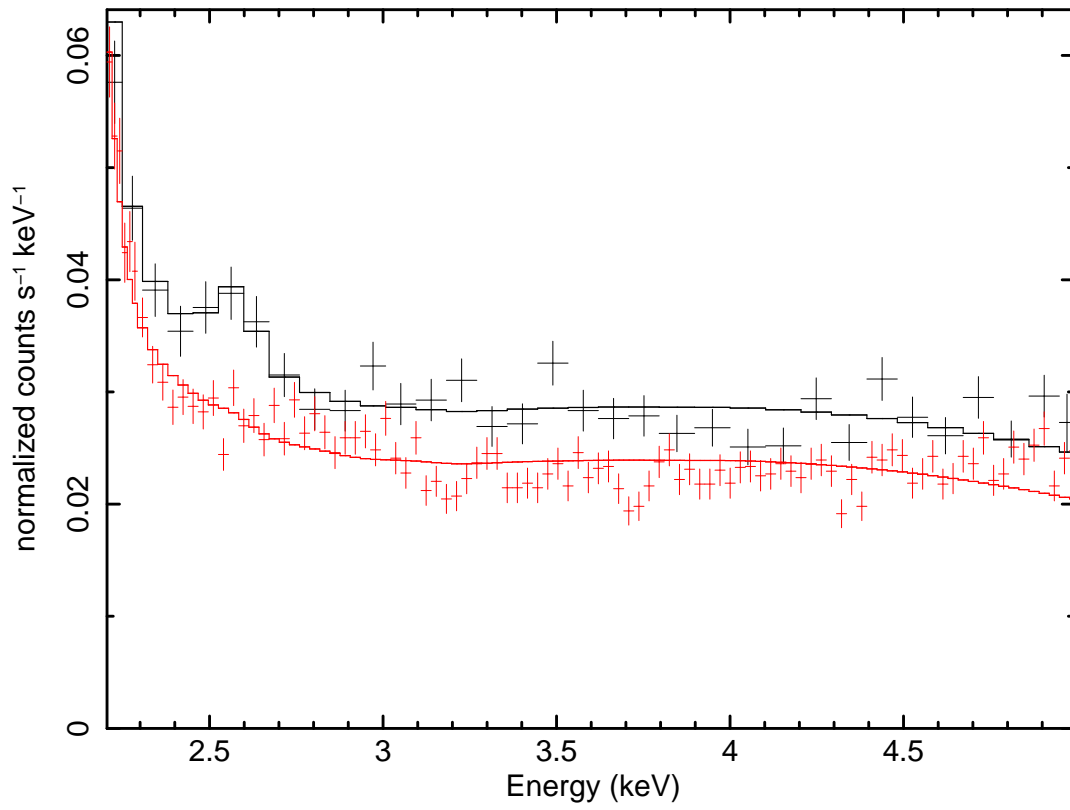


Fig. 12.— Spectra and models from Figure 11, rebinned and plotted together.

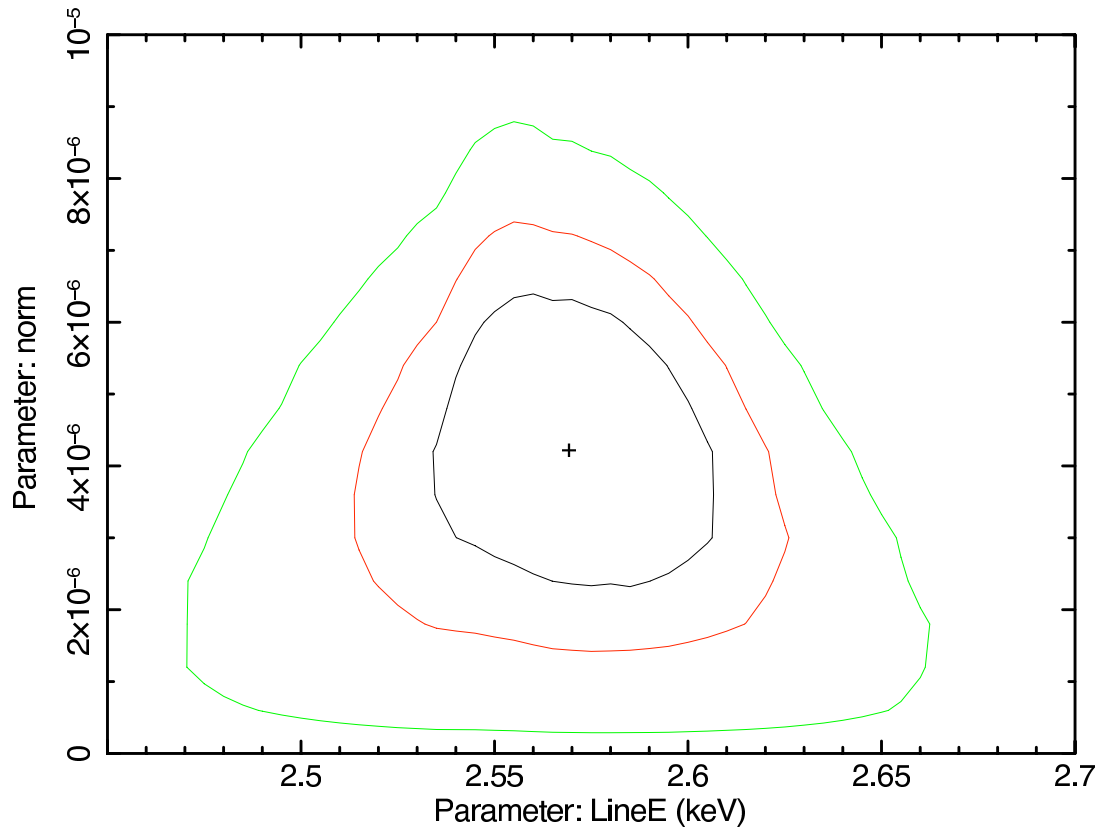


Fig. 13.—  $\Delta C = 2.3, 4.61,$  and  $9.21$  confidence contours for the emission line parameters in fits to the unsubtracted, unbinned Willman 1 spectrum.

That is, the current absence of other positive detections may, in every case, be accommodated with confirmation of the Willman 1 provisional detection reported here – given the uncertainties in mass profiles and various other factors discussed in this section. Our measurement lies near the limit of faint source line fluxes attainable with the best current detectors and, even in the most promising targets, the possible presence of sterile neutrinos with the most suitable parameters in terms of viability as a dark matter candidate lie tantalizingly close to the edge of detectability. It is notable that the Willman 1 X-ray observation is unique in that it represents the only deep *Chandra* exposure of a very high mass-to-light system, so that all sources of competing 2.5 keV line and continuum emission of astrophysical origin are minimized. On the other hand, the dynamical nature of Willman 1 remains unresolved and continues to be investigated (Gutowski et al. 2010; Willman 2010). Additional observations of this – and/or other similar – dwarf spheroidals may be required to settle the question of whether the Willman 1 feature is real or spurious.

## 5. Implications of a Detection

One can take two different approaches to interpreting the spectral line from a decaying relic particle. If one assumes dark matter is solely composed of sterile neutrinos, then the number density of particles is determined by the particle mass and the mixing angle is inferred from the line flux. Alternatively, one can relax the assumption equating the relic density and total dark matter density (Hinshaw et al. 2009) – e.g., there may be additional contributing dark matter components. Regardless of any additional physics, sterile neutrinos of a given mass and mixing angle are produced by neutrino oscillations (Dodelson & Widrow 1994) at a rate that is calculable and cannot be reduced by any unknown high-scale physics.<sup>5</sup> The contours for the allowed ranges of mass and mixing angle are somewhat different depending on whether the relic sterile neutrino density is assumed to be equal to the measured cosmological density of dark matter (Kusenko 2006). We show the results of both approaches in Figure 14.

Interpreted as a sterile neutrino radiative decay, the emission line energy and 90% flux limits imply  $m_{\text{st}} = 5 \pm 0.2$  keV,  $\Gamma_{\nu_s \rightarrow \gamma \nu_a} = (1.4 \pm 1.1) \times 10^{-27} (f_{\text{st}} M_7 / 0.2)^{-1}$ , and  $\sin^2 \theta = (7.8 \pm 6.1) \times 10^{-10} (f_{\text{st}} M_7 / 0.2)^{-1}$ , where the projected mass in the *Chandra* beam is normalized to the fiducial value of  $2 \times 10^6 M_\odot$ .  $\sin^2 \theta = 1.7 \times 10^{-10} (M_7 / 0.2)^{-1}$  represents an absolute lower limit to the mixing angle, regardless of the sterile neutrino production mechanism. If

---

<sup>5</sup>The only caveat to this argument is the possibility of a non-standard cosmology with a low reheat temperature, as pointed out by Gelmini et al. (2004).

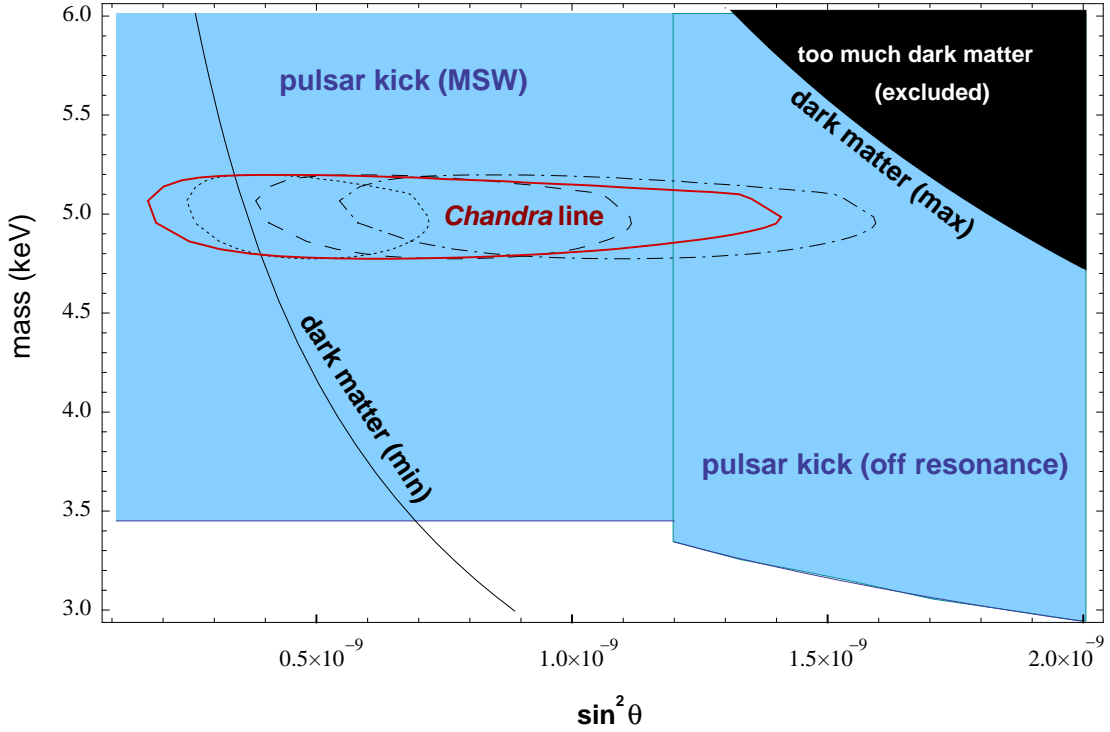


Fig. 14.— For sterile neutrinos that make up 100% of dark matter, the allowed range for the mass and the mixing angle inferred from the *Chandra* data is shown by the solid contour. This range is consistent with the region corresponding to production by non-resonant oscillations alone that is circumscribed by the solid lines marked “dark matter (min)” and “dark matter (max)”. If the primordial abundance of sterile neutrinos is not assumed, the allowed range for the mass and the mixing angle is shown by dotted, dashed, and dot-dashed contours corresponding to maximum, average, and minimum efficiency production by neutrino oscillations. A projected mass within 55 pc of  $2 \times 10^6 M_{\odot}$  is assumed (Strigari et al. 2008b). The inferred parameters are consistent with the pulsar kick mechanisms based on either resonant (MSW) or non-resonant production in the cooling neutron star (see text, Kusenko 2009).

there was some DW production, at least  $9.5(M_7/0.2)^{-1}\%$  of the dark matter must have been produced in this manner (based on the minimum production and lower line flux limit). If the DW mechanism is responsible for all of the sterile neutrino production,  $\sin^2 \theta = (2.5 - 15.7) \times 10^{-10}(M_7/0.2)^{-1/2}$ , where the lower (upper) limit corresponds to the line flux lower (upper) limit and the maximum (minimum) production; and,  $f_{\text{st}} > 0.31(M_7/0.2)^{-1/2}$ . The data is consistent with DW production and  $f_{\text{st}} = 1$  (Figure 9) for  $M_7 = 0.019 - 0.77$ , where the lower (upper) limit is derived from the minimum (maximum) flux and production. The corresponding mixing angle for minimum (maximum) production is  $\sin^2 \theta = 17.7(3.6) \times 10^{-10}$ . In fact our best fit flux matches that expected for average DW production and  $f_{\text{st}} = 1$  for  $M_7 = 0.18$  ( $\sin^2 \theta = 8.2 \times 10^{-10}$ ), which is close to our fiducial mass (Figure 9).

The allowed region may be further circumscribed if combined with previously derived constraints. Limits have been derived using a variety of datasets (mostly based on *Chandra* or *XMM-Newton* data), employing a variety of data reduction, background mitigation, and statistical techniques to derive upper limits, taking diverse approaches (if any) to account for emission associated with baryons (see above), and depend on different methods for estimates (and associated uncertainties) of the dark matter content in the field-of-view. The limits based on *Chandra* deep field measurements of the unresolved X-ray background originating in the Milky way dark matter halo (Abazajian et al. 2007) are perhaps the most directly comparable in that deep *Chandra* ACIS-I data (some of which was taken in VFAINT mode) was utilized. These constraints are consistent with dark matter being composed of  $m_{\text{st}} = 5$  keV sterile neutrinos produced by the DW mechanism. *XMM-Newton* observations of diffuse emission in the M31 halo are formally inconsistent with our best-fit flux under the same assumptions. However, taking the uncertainties into account, an ample region of concordance is retained that includes parameters where  $f_{\text{st}} = 1$  and non-resonant oscillations are the dominant, or sole, mechanism of sterile neutrino production (Section 4.2).

This interpretation has immediate implications for particle physics and astrophysics. In particular, supernova physics is altered dramatically by the emission of a 5 keV sterile neutrino that has a mixing angle  $\sin \theta \sim 10^{-5} - 10^{-4}$ . First, the emission is anisotropic, with the direction of anisotropy set by the electron spins polarized in the magnetic field (Kusenko & Segrè 1997; Fuller et al. 2003). While the overall energy removed by sterile neutrinos with 5 keV mass and  $\sin \theta \sim 10^{-5} - 10^{-4}$  is small, the anisotropy in the emission of sterile neutrinos plays a central role in generating the supernova asymmetries. Second, the lepton number, energy, and entropy transport in the cooling neutron star are affected, and an increase in the electron neutrino luminosity can preheat the material in front of the shock wave, adding to the energy of the overall explosion (Hidaka & Fuller 2007). Third, the neutrino-driven kick enhances the convection in front of the neutron star, which causes some energy increase of the shock wave (Fryer & Kusenko 2006). The numerical simulations of this effect show the

formation of asymmetric jets with the stronger jet pointing in the direction of the pulsar motion (Fryer & Kusenko 2006).

From the point of view of particle physics, the 5 keV sterile neutrino with a small mixing angle can be accommodated in a seesaw mass matrix that satisfies all the experimental and observational constraints (Kusenko 2009). The values inferred from the *Chandra* observations allow for all dark matter to be produced via neutrino oscillations, so that no additional production mechanism is necessary. This, however, does not preclude the 5 keV mass from being generated via the Higgs mechanism by a vacuum expectation value of an electroweak-scale singlet Higgs boson, which may be discoverable by upcoming experiments at the Large Hadron Collider (Kusenko 2006; Petraki & Kusenko 2008).

The X-rays emitted by dark matter decay during the “dark ages” could produce a strong enough ionization to enhance the formation of molecular hydrogen, which, in turn, could speed up the formation of the first stars (Biermann & Kusenko 2006). The corresponding predictions for 21 cm and other observations depend on the knowledge of the particle mass and mixing angle (Stasielak et al. 2007) that are greatly refined if the dark matter particle has the mass and mixing inferred from *Chandra* observations of Willman 1.

Finally, there is no doubt that observational cosmology will take advantage of our finding if it is confirmed. If dark matter emits a narrow spectral line in X-rays, one can hope to map out the three-dimensional dark matter distribution, including the redshift, using future X-ray telescopes such as *Astro-H*<sup>6</sup> and *IXO*.<sup>7</sup> Such data could be used to study the expansion of the universe on cosmological distance scales.

## 6. Summary and Concluding Remarks

We presented results of a search for a radiatively decaying dark matter emission line in the *Chandra* spectrum of the ultra-faint dwarf spheroidal galaxy Willman 1.  $\Delta\chi^2 = 9.2$  upper limits on the line flux over the 0.4-7 keV bandpass were translated to an allowed region in the sterile neutrino mass-mixing angle plane for the case where all of the dark matter is composed of sterile neutrinos regardless of how they are produced, and in the more general case where their abundance is not assumed but is calculated under the assumptions that minimize it. These constraints are consistent with and therefore, given the uncertainties in mass determination, reinforce those derived from previous X-ray analysis of dwarf spheroidal

---

<sup>6</sup><http://heasarc.gsfc.nasa.gov/docs/astroh/>, <http://astro-h.isas.jaxa.jp/>

<sup>7</sup><http://ixo.gsfc.nasa.gov/>

galaxies (LKB, Riemer-Sorensen & Hansen 2009).

We uncovered evidence of an emission line in the Willman 1 X-ray spectrum with energy  $2.51 \pm 0.07(0.11)$  keV and flux  $[3.53 \pm 1.95(2.77)] \times 10^{-6}$  photons  $\text{cm}^{-2} \text{s}^{-1}$ , where the errors are 68% (90%) confidence limits. This was based on an excess to the continuum measured by fitting the particle-background-subtracted source spectrum, where the VFAINT data-mode quiescent background reduction technique was applied. Consistent parameters were found using maximum likelihood fitting to the unbinned, unsubtracted spectrum. Re-examination of *Suzaku* data of the Ursa Minor dwarf spheroidal, and *Chandra* data on the Draco dwarf spheroidal, reveal a possible confirmation in the *Suzaku* XIS1 spectrum of Ursa Minor, but not in any of the other spectra. Evidence of dark matter radiative decay in Willman 1 remains provisional due to the low level of significance, but uncontradicted. In the short term, additional X-ray observations of SDSS dwarf spheroidals are needed, while future high energy resolution X-ray spectroscopy should prove definitive.

We derive the range of allowed sterile neutrino mass and mixing angle implied by the 90% confidence limits of line energy and flux, assuming that either (1) dark matter solely consists of sterile neutrinos regardless of how they are produced, or that (2) they are solely produced by neutrino oscillations regardless of whether the abundance matches that of dark matter as inferred from cosmology. Remarkably, the two allowed regions strongly overlap – that is, the observations are consistent with the narrow region in the mass-mixing-angle plane where neutrino oscillations may produce all of the dark matter (although it allows for some non-DW production). Moreover, the inferred parameters are consistent with the pulsar kick mechanisms based on either resonant or non-resonant sterile neutrino production in cooling neutron stars. This unlikely concordance intensifies the importance and urgency of additional investigation.

The authors thank James Bullock and Manoj Kaplinghat for discussions of mass profiles, target selection, and other key issues related to this work. We are also grateful to Beth Willman for providing the latest information on the nature of Willman 1, the referee for a thorough and constructive report, and members of the astroparticle physics community too numerous to name for feedback via e-mail and at scientific meetings. Support for this work was provided by the National Aeronautics and Space Administration through *Chandra* Award Numbers G08-9091X and G09-0090X issued by the Chandra X-ray Observatory Center, which is operated by the Smithsonian Astrophysical Observatory for and on behalf of the National Aeronautics Space Administration under contract NAS8-03060. The work of AK was supported in part by DOE grant DE-FG03-91ER40662 and NASA ATFP grant NNX08AL48G.

## REFERENCES

- Abazajian, K., Fuller, G. M., & Patel, M. 2001, *Phys. Rev. D*, 64, 023501
- Abazajian, K., Fuller, G. M., & Tucker, W. H. 2001, *ApJ*, 562, 593
- Abazajian, K. N., Markevitch, M., Koushiappas, S. M., & Hickox, R. C. 2007, *Phys. Rev. D*, 75, 063511
- Asaka, T., Shaposhnikov, M., & Laine, M. 2007, *JHEP*, 01, 091
- Barger, V., Phillips, R. J. N., & Sarkar, S. 1995, *Physics Letters B*, 352, 365; erratum *ibid.* 356, 617.
- Biermann, P. L., & Kusenko, A. 2006, *Physical Review Letters*, 96, 091301
- Bogdan, A., & Gilfanov, M. 2008, *MNRAS*, 388, 56
- Boyanovsky, D. 2008, *Phys. Rev. D*, 77, 023528
- Boyanovsky, D. 2008, *Phys. Rev. D*, 78, 103505
- Boyarsky, A., Neronov, A., Ruchayskiy, O., Shaposhnikov, M., & Tkachev, I. 2006, *Physical Review Letters*, 97, 261302
- Boyarsky, A., Iakubovskiy, D., Ruchayskiy, O., Savchenko, V. 2008, *MNRAS*, 387, 136
- Boyarsky, A., Lesgourgues, J., Ruchayskiy, O., & Viel, M. 2009, *Physical Review Letters*, 102, 201304
- Boyarsky, A., Ruchayskiy, O., Iakubovskiy, D., Walker, M. G., Riemer-Sorensen, S., & Hansen, S. H. 2010, *arXiv:1001.0644*
- Burkert, A. 1995, *ApJ*, 447, L25
- Chemin, L., Carignan, C., & Foster, T. 2009, *ApJ*, 705, 1395
- Corbelli, E., Lorenzoni, S., Walterbos, R. A. M., Braun, R., & Thilker, D. A. 2009, *arXiv:0912.4133*
- Cash, W. 1979, *ApJ*, 228, 939
- Chartas, G., et al. 2000, *ApJ*, 542, 655
- Churazov, E., Forman, W., Vikhlinin, A., Tremaine, S., Gerhard, O., & Jones, C. 2008, *MNRAS*, 388, 1062

- Dodelson, S., & Widrow, L. M. 1994, *Phys. Rev. Lett.*, 72, 17
- Dolgov, A. D., & Hansen, S. H. 2002, *Astroparticle Physics*, 16, 339
- Fryer, C. L., & Kusenko, A. 2006, *ApJS*, 163, 335
- Fuller, G. M., Kusenko, A., Mocioiu, I., & Pascoli, S. 2003, *Phys. Rev. D*, 68, 103002
- Gelmini, G., Palomares-Ruiz, S., & Pascoli, S. 2004, *Physical Review Letters*, 93, 081302
- Gutowski, G., et al. 2010, *BAAS*, 215, 457.01
- Hidaka, J., & Fuller, G. M. 2007, *Phys. Rev. D*, 76, 083516
- Hinshaw, G., et al. 2009, *ApJS*, 180, 225
- Kusenko, A. 2006, *Physical Review Letters*, 97, 241301
- Kusenko, A. 2009, *Phys. Rept.*, 481, 1 (K09)
- Kusenko, A., and Loewenstein, M. 2010, arXiv:1001.0644
- Kusenko, A., & Segrè, G. 1997, *Physics Letters B*, 396, 197
- Li, Z., & Wang, Q.D. 2007, *ApJ*, 668, L39
- Loewenstein, M., Kusenko, A., & Biermann, P. L. 2009, *ApJ*, 700, 426 (LKB)
- Maccarone, Thomas J.; Kundu, Arunav; Zepf, Stephen E.; Piro, Anthony L.; Bildsten, L. 2005, *MNRAS*, 364, L61
- Matsumoto, H., Koyama, K., Awaki, H., Tomida, H., Tsuru, T., Mushotzky, R., & Hatsukade, I. 1996, *PASJ*, 48, 201
- Mushotzky, R. F., Cowie, L. L., Barger, A. J., & Arnaud, K. A. 2000, *Nature*, 404, 459
- Navarro J. F., Frenk C. S., & White S. D. M. 1997, *ApJ*, 490, 493
- Pal, P. B., & Wolfenstein, L. 1982, *Phys. Rev. D*, 25, 766
- Petraki, K. 2008, *Phys. Rev. D*, 77, 105004
- Petraki, K., & Kusenko, A. 2008, *Phys. Rev. D*, 77, 065014
- Revnivtsev, M., Churazov, E., Sazonov, S., Forman, W., & Jones, C. 2008, *A&A*, 490, 37
- Riemer-Sorensen, S.; Hansen, S. H. 2009, *A&A*, 500, L37

- Saglia, R. P., Fabricius, M., Bender, R., Montalto, M., Lee, C. -H., Riffeser, A., Seitz, S., Morganti, L., Gerhard, O., & Hopp, U. 2010, A&A, in press (arXiv:0910.5590)
- Shaposhnikov, M., & Tkachev, I. 2006, Physics Letters B, 639, 414
- Shi, X., & Fuller, G. M. 1999, Physical Review Letters, 82, 2832
- Stasielak, J., Biermann, P. L., & Kusenko, A. 2007, ApJ, 654, 290
- Strigari, L. E., Bullock, J. S., & Kaplinghat, Diemand, J., Kuhlen, M., & Madau, P. 2007, ApJ, 669, 676
- Strigari, L. E., Bullock, J. S., Kaplinghat, M., Simon, J. D., Geha, M., Willman, B., & Walker, M. G. 2008a, Nature, 454, 1096
- Strigari, L. E., Koushiappas, S. M., Bullock, J. S., Kaplinghat, M., Simon, J. D, Geha, M., & Willman, B. 2008b, ApJ, 678, 614
- Walker, M. G., Mateo, M., Olszewski, E. W., Peñarrubia, J., Wyn Evans, N., & Gilmore, G. 2009, ApJ, 704, 1274
- Watson, C. R., Beacom, J. F., Yüksel, H., & Walker, T. P. 2006, Phys. Rev. D, 74, 033009
- Willman, B. 2010, private communication
- Wolf, J., Martinez, G. D., Bullock, J. S., Kaplinghat, M., Geha, M., Munoz, R. R., Simon, J. D., & Avedo, F. F. 2009, MNRAS, submitted
- Xue et al. 2008, ApJ, 684, 1143
- Yaqoob, T. 1998, ApJ, 500, 89